Title: Crystallinity modulated electrocatalytic activity of nickel(II) borate thin layer on Ni3B for efficient water oxidation

Authors: Wen-Jie Jiang; Shuai Niu; Tang Tang; Qin-Hua Zhang; Xiao-Zhi Liu; Yun Zhang; Yu-Yun Chen; Jihui Li; Lin Gu; Li-Jun Wan; Jinsong Hu

To be cited as: 10.1002/ange.201703183

Link to VoR: https://doi.org/10.1002/ange.201703183

Crystallinity modulated electrocatalytic activity of nickel(II) borate thin layer on Ni_3B for efficient water oxidation

Wen-Jie Jiang, Shuai Niu, Tang Tang, Qing-Hua Zhang, Xiao-Zhi Liu, Yun Zhang, Yu-Yun Chen, Ji-Hui Li, Lin Gu,* Li-Jun Wan, and Jin-Song Hu*

Abstract: The exploration of new efficient non-precious OER electrocatalysts and the understanding the relationship between activity and structure of electrocatalysts are important to advance electrochemical water oxidation. Herein, we developed an efficient OER electrocatalyst with inner nickel boride (Ni_3B) nanoparticles as cores and nickel (II) borate (Ni-B_i) as shells (Ni-B_i@NB) via a very simple and facile aqueous reaction, which exhibited a small overpotential of 302 mV at 10 mA cm^{-2} and Tafel slope of 52 mV/decade. More interestingly, it was found that the OER activity of Ni-B_i@NB was closely dependent on the crystallinity of Ni-B_i shells. The partially crystalline Ni-B_i exhibited the much higher activity than amorphous or crystalline one, which originated from the enhanced intrinsic activity of catalytic sites. These findings open up opportunities to explore nickel (II) borates as a new class of efficient non-precious OER electrocatalysts, and to improve the electrocatalyst performance by modulating their crystallinity.

Hydrogen as a carbon-free fuel with high energy density has been considered as an ideal energy carrier alternative to current fossil fuels for meeting the global rapidly-growing energy demand and environmental concerns. One environmentally friendly and practical approach to produce hydrogen is water electrolysis[1]. However, oxygen evolution reaction (OER) at the anode of water electrolyzer limits the efficiency of water splitting due to the high overpotential and usually needs noble metal catalysts such as RuO_2 and IrO_2.[1] Therefore, it is necessary to develop earth-abundant non-precious OER catalysts for practical water electrolysis.[2] Among them, nickel-based oxides and (oxy)hydroxides have been well-explored and shown outstanding performance for OER[3]. These conventional non-precious electrocatalysts have achieved a current density of 10 mA cm^{-2} at operating overpotential in the range of 0.35 to 0.43.[4] Such catalytic properties could be further enhanced by the introduction of additional transition metals, such as Fe and Co, to produce spinels or layered double hydroxides.[5] In past several years, metal (including nickel, cobalt, iron, and manganese) compounded with elemental sulfur,[6] selenium,[7] phosphor,[8] nitrogen,[9] and boron[10] have been also investigated as the potential OER electrocatalysts. Some of them exhibited the electrocatalytic performances comparable to or even better than traditional nickel oxides, (oxy)hydroxides and commercial RuO_2, IrO_2. To expand the scope of non-precious OER catalysts with the potential for large-scale applications, the development of new efficient non-precious electrocatalysts and the understanding the relationship between activity and structure of catalysts are still intriguing and important.

In the family of metal (Co and Ni) phosphate and borate OER catalysts, Nocera et. al. explored cobalt phosphate (Co(III)-P_i) as oxygen evolution catalyst in artificial system of water splitting driven by solar light in 2008.[11] Subsequently, they demonstrated that the electrodeposited cobalt (III) phosphate film could be also used for electrocatalytic water oxidation with an overpotential down to 345 mV.[12] Very recently, a hybrid of Co(II)-borate (B_i) ultrathin nanosheets and graphene was developed by Xie et al. as an efficient OER electrocatalyst.[13] Similar to Co-P_i and -B_i, Nocera et al. reported that the electrodeposited Ni(III)-B_i film exhibited electrocatalytic activity for oxygen evolution in borate electrolyte,[14] and further discovered that the anodic activation of Ni(III) to Ni(III/IV) dramatically increased the OER activity of the electrodeposited Ni(III)-B_i film in near neutral regimes.[15] Up to now, nickel-based borates have never been reported for OER in strongly alkaline medium which is more attractive and compatible with the current industrial applications. Moreover, it has been demonstrated that the electrocatalysts in amorphous state usually exhibited better activity over that in crystalline state.[16] Deliberately tuning the crystalline degree of electrocatalysts and investigating its influence on electrocatalytic activity would offer an alternative way to improve the electrochemical performance, which was rarely reported yet and might open opportunities to achieve efficient electrocatalysts.

Herein, we report a new efficient OER electrocatalyst with the core-shell structure of Ni(II)-B_i shell on nickel boride (NB) nanoparticle cores (Ni-B_i@NB) prepared by a very simple aqueous reaction. It is intriguingly found that the OER electrocatalytic activity can be modulated by controlling the crystallinity of Ni(II)-B_i shell. The amorphous Ni-B_i@NB (a-Ni-B_i@NB) requires an overpotential of 364 mV at 10 mA cm^{-2} for OER in 1 M KOH electrolyte, while the partially crystalline Ni-B_i@NB (pc-Ni-B_i@NB) exhibits a significantly enhanced OER activity with an overpotential of only 302 mV, which is 23 mV less than commercial IrO_2 catalyst. However, further increasing the crystallinity of Ni-B_i shell unfavorably downgrades its OER

[a] W.-J. Jiang,[+] S. Niu,[+] T. Tang, Y. Zhang, Y.-Y. Chen, Prof. L.-J. Wan, Prof. J.-S. Hu
Key Laboratory of Molecular Nanostructure and Nanotechnology
Institute of Chemistry, Chinese Academy of Science
Beijing 100190 (China)
E-mail: hujs@iccas.ac.cn
Q.-H. Zhang, W.-Z. Liu, Prof. L. Gu
Beijing National Laboratory for Condensed Matter Physics
Institute of Physics, Chinese Academy of Science
Beijing 100019 (China)
E-mail: l.gu@iphy.ac.cn
S. Niu, Prof. J.-H. Li
College of Chemistry and Material Science, Hebei Normal Univeristy, Shijiazhuang 050024 (China)
W.-J. Jiang, Prof. L.-J. Wan, Prof. J.-S. Hu
University of the Chinese Academy of Sciences
Beijing 100049 (China)

[+] These authors contributed equally to this work.

Supporting information for this article is given via a link at the end of the document

activity. The quantitative analyses of the turnover of frequencies (TOF) per oxidative nickel atom for a-Ni-B_i@NB and pc-Ni-B_i@NB reveal that TOF of pc-Ni-B_i@NB is 0.052 s^{-1} at the overpotential of 300 mV, which is nearly seven times higher than for a-Ni-B_i@NB (0.008 s^{-1}). Therefore, the significantly enhanced performance should be ascribed to the much higher intrinsic OER catalytic activity of partially crystalline Ni-B_i than amorphous or crystalline Ni-B_i. Together with the low Tafel slope of 52 mV/decade, the present pc-Ni-B_i@NB outperforms most conventional Ni-based oxides,[8a] sulfides,[6a] hydroxides,[3, 5d] and is in line with the current benchmark OER electrocatalysts such as newly reported nickel-based phosphides[8a] and layered double hydroxides.[5e] These findings could inspire the further development of three-dimensional nanostructured Ni-B_i-based materials towards a new class of non-precious efficient OER electrocatalysts.

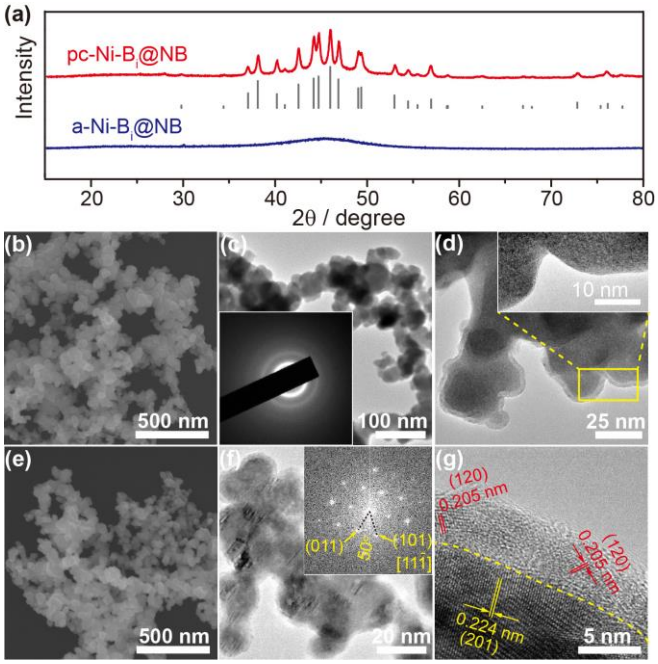

Figure 1. (a) XRD patterns of a-Ni-B_i@NB and pc-Ni-B_i@NB. (b) SEM and (c,d) TEM images of a-Ni-B_i@NB. The inset in c is SAED pattern. The inset in d is HRTEM image on selected area. (e) SEM, (f) TEM and (g) HRTEM images of pc-Ni-B_i@NB. The inset in f is FFT pattern of an individual Ni_3B nanocrystal.

Amorphous a-Ni-B_i@NB was firstly synthesized by a simple and cost-effective method using the aqueous reaction of $Ni(ac)_2$ and $NaBH_4$ at room temperature. Typical partially crystalline pc-Ni-B_i@NB was obtained through annealing a-Ni-B_i@NB at 350 ^oC in Ar for 2 h (see supporting information (SI) for details). About 4 g pc-Ni-B_i@NB can be easily obtained in one batch synthesis with ~100% conversion of Ni precursor (Figure S1). X-ray diffraction (XRD) pattern of the as-obtained a-Ni-B_i@NB (blue curve in Figure 1a) indicates its amorphous nature in terms of a broad peak. After annealing, XRD pattern (red curve) exhibits distinct XRD peaks. All these peaks can be assigned to Ni_3B (JCPDS No. 48-1223, gray vertical lines), clearly suggesting the appearance of Ni_3B. No signals of crystallized Ni-B_i was observed in the XRD pattern, which could be due to the low content and low crystallinity of Ni-B_i in the sample (Figure S2). Their morphologies were then investigated by scanning electron microscopy (SEM) and transmission electron microscopy (TEM). As shown in Figure 1b and 1c, a-Ni-B_i@NB shows interconnected nanoparticles with a mean size of 44 nm (Figure S3). The diffuse rings in the selected area electron diffraction (SAED) pattern confirm the amorphous nature of these nanoparticles. The energy dispersive X-ray spectrum (EDS) reveals that the sample is composed of Ni (79.06 at. %), B (15.39 at. %) and O (5.55 at. %), indicating a-Ni-B_i@NB is of Ni-rich (Figure S4 and Table S1). A close look (Figure 1d) clearly shows a thin layer in ~ 4 nm is uniformly coated on amorphous nanoparticles. This thin layer is very sensitive to the electron beam and disappears during high-resolution TEM (HRTEM) observation (inset in Figure 1d), similar to the report about unstable Ni-B_i prepared through similar method.[17] Referring to the previous studies,[18] these results indicate that the inside nanoparticles should be amorphous nickel borides (Ni_xB) and the outlayer should be amorphous nickel borate (Ni-B_i). To explore the formation process of a-Ni-B_i@NB core-shell structure, the reaction kinetics was slowed by reducing the concentration of $NaBH_4$ reductant from 1 M to 0.01 M and simultaneously the reaction temperature to 0 ^oC using ice-water bath. As shown in the TEM image (Figure S5), Core-shell structure could be clearly observed immediately after adding $NaBH_4$ into $Ni(ac)_2$ aqueous solution, indicating that the formation of core-shell structure and the reduction of nickel cations might proceed almost at the same time. It is known that $NaBH_4$ can hydrolyze to borate anions, which will instantly compound with nickel cations to form Ni-B_i. Metal borides can catalyze the hydrolysis of $NaBH_4$ so that Ni-B_i will preferably form surrounding the newly-formed nickel boride nanoparticles, leading to the Ni-B_i@NB core-shell structure. After annealing at 350 ^oC in Ar, the nanoparticles slightly shrink as evidenced in SEM and TEM images (Figure 1e, 1f and Figure S6). The mean size of nanoparticles decreased to 37 nm for pc-Ni-B_i@NB (Figure S3). The thermogravimetric analysis shows only 1.17% mass loss during the annealing (Figure S7). Fast Fourier transformed (FFT) pattern taken on an individual nanoparticle (inset in Figure 1f) during TEM observation shows ordered bright spot array with the features of N_3B, indicative of crystalline nature of the inner nanoparticle. The continuous lattice distance of 0.224 nm in HRTEM image (Figure 1g) is well consistent with the d-spacing of (201) crystallographic planes of Ni_3B. In contrast to a-Ni-B_i@NB, the sensitive disordered amorphous shell converted into partially crystalline structure with lattice fringes in short-range and became robust under electron irradiation. The lattice spacing of 0.205 nm matches well with the d-spacing of (120) crystallographic planes of Ni-B_i ($Ni_3(BO_3)_2$, JCPDS No. 75-1809). Together with the XRD analysis, these results reveal that annealing process turns amorphous Ni_xB into well-crystallized Ni_3B and amorphous Ni-B_i into partially crystalline Ni-B_i (pc-Ni-B_i).

It is known that the surface composition and chemical state dominate the electrocatalytic performance of an electrocatalyst. X-ray photoelectron spectroscopy (XPS) were performed to identify the surface chemical states of a-Ni-B_i@NB and pc-Ni-

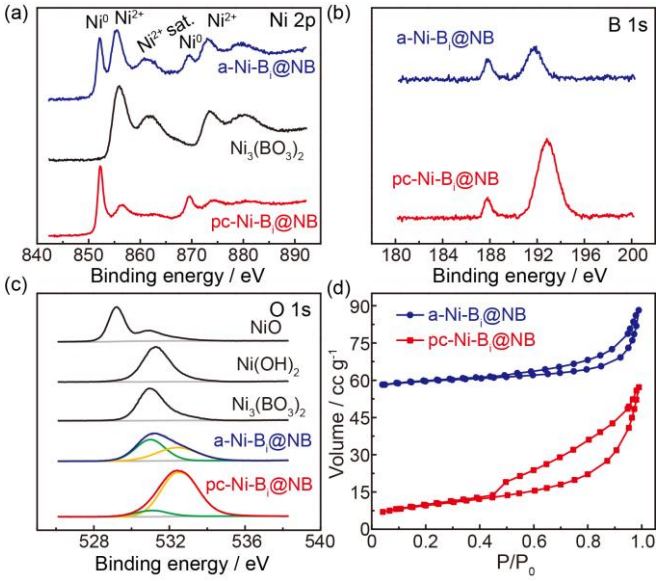

Bi@NB. As shown in Figure 2a, both two samples show two distinct peaks of Ni $2p_{3/2}$ core level. The peak at the low binding energy of 852.2 eV can be assigned to metallic Ni^0,[19] originating from the inner Ni_xB nanoparticles in view of the sampling depth of XPS (about 10 nm). Another peak at the higher binding energy

Figure 2. (a) Ni 2p, (b) B 1s and (c) O 1s XPS spectra of a-Ni-B_i@NB, pc-Ni-B_i@NB and the references. (d) Nitrogen adsorption-desorption isotherms of a-Ni-B_i@NB and pc-Ni-B_i@NB.

(855.4 eV for a-Ni-B_i@NB and 856.6 eV for pc-Ni-B_i@NB) are close to that of Ni^{2+} signal.[20] Furthermore, the bivalent nickel in Ni-B_i shell was verified by the L_3/L_2 area ratio in Ni-L spectra of electron energy loss spectroscopy (EELS) which is very sensitive to the chemical valence of metal (see Figure S8 for experimental details and discussion).[21] No clear the signal of Ni^{3+} is detected in both products. The difference of Ni^{2+} between these two binding energies can be attributed to the electron transfer from elemental B to the empty *d* orbits of Ni after annealing, resulting in the enriched electrons in Ni but deficient electrons in B.[22] Apart from the signal of Ni^0, the rest profile of Ni 2p spectra of both samples are very similar to that in nickel borate (black curve), corroborating the presence of nickel borate on surface. The Ni $2p_{3/2}$ spectra were further deconvoluted to quantify the amount of oxidative Ni species (Figure S9). Ni^{2+} decreases significantly from 14.91 at.% in a-Ni-B_i@NB to 3.88 at.% in pc-Ni-B_i@NB, indicating the relative amount of nickel borate on surface decreases after annealing (Figure S10). The B1s spectra of both samples show two distinct peaks (Figure 2b). The former peak at 187.7 eV can be assigned to B signal in Ni_xB,[10d, 19] indicative of the presence of nickel borides. The one at higher binding energy (191.7 eV for a-Ni-B_i@NB and 192.8 eV for pc-Ni-B_i@NB) can be attributed to the B-O bonding in borate or boron oxide.[13] The O1s spectra (Figure 2c) of both samples as well as NiO, $Ni(OH)_2$ and nickel borate as references were also analyzed. O1s spectrum of a-Ni-B_i@NB and pc-Ni-B_i@NB could be decconvoluted into two peaks at 531.0 and 532.5 eV, corresponding to the binding energy of B-O-Ni in Ni-B_i and B-O bonds in B_2O_3.[22-23] The relative content of B-O-Ni specie decreases appreciably in pc-Ni-B_i@NB, which is consistent with the variation of Ni^{2+} (Figure 2a). The above results disclose that the relative content of Ni-B_i on the surface of pc-Ni-B_i@NB decrease compared with a-Ni-B_i@NB. Concomitantly, quantitative analyses on the atomic ratios of Ni : B in bulk (EDS) and on surface (XPS) demonstrate that both catalysts are of Ni-rich in bulk and B-rich on surface (Table S1). Therefore, it can be concluded that the annealing turns inner amorphous Ni_xB into crystalline Ni_3B, accompanying with the outmigration of B and formation of B_2O_3 in the outlayer of Ni_3B nanoparticles which causes the decrease in the relative content of Ni-B_i. When the annealing temperature was further increased to 450 °C, it was found that the inner amorphous Ni_xB was fully transformed into metallic Ni as evidenced by the XRD pattern in Figure S11. This fact corroborates the outmigration of B during annealing. Moreover, the N_2 isothermal adsorption measurements (Figure 2d) show that the total specific surface area (SSA) calculated by Brunauer-Emmett-Teller (BET) method is 12.9 $m^2\ g^{-1}$ and 26.4 $m^2\ g^{-1}$ for a-Ni-B_i@NB and pc-Ni-B_i@NB, respectively.

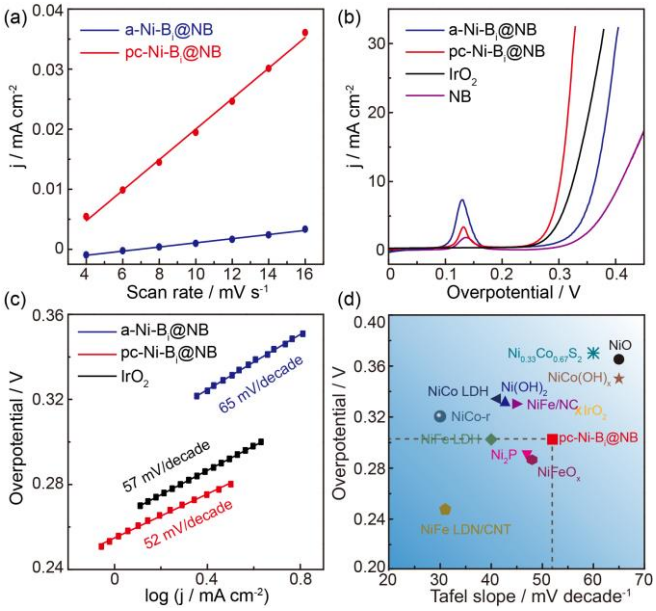

Figure 3. (a) Current density as a function of scan rates. (b) Polarization curves and (c) corresponding Tafel plots of a-Ni-B_i@NB, pc-Ni-B_i@NB, NB and commercial IrO_2 in 1 M KOH. (d) Overpotential at 10 mA cm^{-2} and Tafel slope of the state-of-the-art OER electrocatalysts supported on glass carbon electrode in 1 M KOH (Table S2). The influence of the different nanostructures of these catalysts on catalytic performance is not considered.

To investigate electrocatalytic OER activities of as-prepared a-Ni-B_i@NB and pc-Ni-B_i@NB, the catalysts were deposited onto a glass carbon electrode (GCE) with a loading of 0.3 mg cm^{-2} and evaluated in 1 M KOH. Electrochemically active surface area (EASA) was firstly determined by capacitance measurements via cyclic voltammogram in the double layer region (without faradaic processes) at different scan rates (Figure S12). The calculated capacitance of a-Ni-B_i@NB and pc-Ni-B_i@NB are 0.35 and 2.54 mF cm^{-2}, respectively (Figure 3a).

The EASA of a-Ni-B_i@NB and pc-Ni-B_i@NB are calculated to be 1.10 and 7.98 cm^2, respectively (see supporting information for details). The polarization curves were recorded from linear sweep voltammetry (LSV) tests at a scan rate of 5 mV s^{-1} to get an overpotential at 10 mA cm^{-2} (a metric relevant to solar fuel synthesis), which is usually used to evaluate the OER performance of an electrocatalyst. Commercial IrO_2 catalyst was also tested to accurately evaluate the OER activities of the catalysts. All potentials are iR corrected values unless noted. In Figure 3b, both a-Ni-B_i@NB and pc-Ni-B_i@NB show an anodic peak at around 1.35 V (*vs*. RHE), which could be commonly observed in Ni-based OER electrocatalysts and assigned to the oxidation of Ni^{2+} to Ni^{3+}.[5c, 7b, 23] The a-Ni-B_i@NB requires an overpotential of 364 mV to reach 10 mA cm^{-2}, while this overpotential dramatically reduces to 302 mV for pc-Ni-B_i@NB (313 mV without iR-correction, Figure S13). Both of which are much lower than 409 mV for Ni_3B without Ni-B_i shell (Figure S14), implying the Ni-B_i shell should be responsible for the enhanced OER activity. The corresponding Tafel slope of pc-Ni-B_i@NB is 52 mV/decade, appreciably lower than 65 mV/decade of a-Ni-B_i@NB (Figure 3c), suggesting the improved OER kinetics on Ni-B_i after annealing. Both the Tafel slope and overpotential at 10 mA cm^{-2} of pc-Ni-B_i@NB are better than those of commercial IrO_2 catalyst (57 mV/decade and 325 mV, respectively) and similar to cobalt borate-graphene composite reported recently.[13] Such OER catalytic performance (comparable overpotential to NiFe LDH[5e] and Tafel slope of amorphous $NiFeO_x$[5f]) of partially crystalline nickel borate could outperform a majority of previous Ni-based oxides,[8a] sulfides,[6a] hydroxides[3, 5d] and even match the benchmark electrocatalysts reported very recently, such as nickel phosphides[8a] or layered double hydroxides[5e] (Figure 3d and Table S2). The catalytic activity of pc-Ni-B_i@NB was normalized by catalyst mass loading (Figure S15). It showed that the overpotentials to reach 10, 50 and 100 mA mg^{-1} are 278, 310 and 325 mV, respectively, indicating outstanding OER catalytic performance (Table S3).

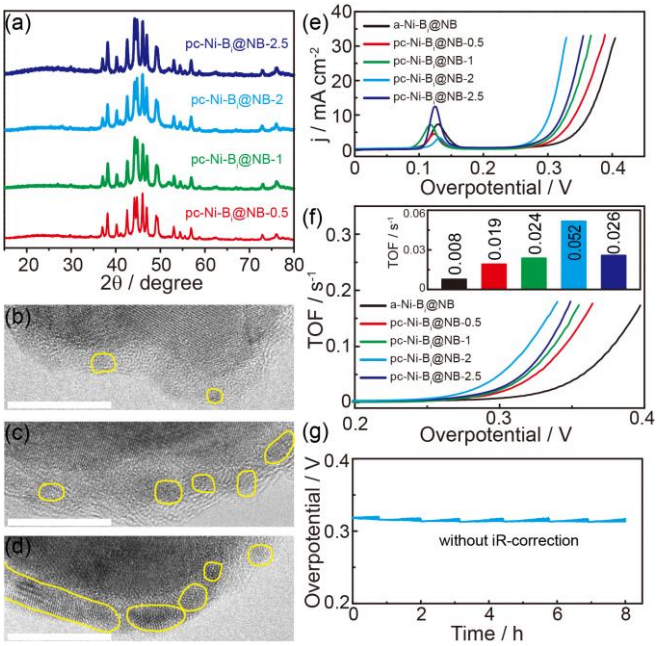

Figure 4. (a) XRD patterns of pc-Ni-B_i@NBs. (b-d) TEM images of pc-Ni-B_i@NB-0.5 (b), pc-Ni-B_i@NB-2 (c) and pc-Ni-B_i@NB-2.5 (d). The scale bars are 10 nm. (e) OER polarization curves and (f) TOF per oxidative nickel site (Ni^{2+}) for a-Ni-B_i@NB and pc-Ni-B_i@NBs. The inset in f is TOF values at the overpotential of 300 mV. (f) Chronopotentiometric curve of pc-Ni-B_i@NB-2 at constant current density of 10 mA cm^{-2}.

It is worthy to point out that B_2O_3 is almost inactive for OER (Figure S16). Given that only Ni-B_i and B_2O_3 exist on the surface of the catalysts, the electrocatalytic OER activities of a-Ni-B_i@NB and pc-Ni-B_i@NB should originate from Ni-B_i, which agrees with the previous investigation by Nocera et. al.[15] The substantial difference in OER performance is suspected to the consequence of the change in the crystallinity of Ni-B_i during annealing. To unravel this point, the crystallinity of Ni-B_i was finely controlled by annealing a-Ni-B_i@NB at 350 ^oC for different dwell time. Besides above-mentioned a-Ni-B_i@NB without annealing and pc-Ni-B_i@NB annealed for 2 h (i.e. pc-Ni-B_i@NB-2), three additional catalysts, pc-Ni-B_i@NB-x (x=0.5, 1, and 2.5, where x stands for the annealing time in hour), were prepared in parallel. Figure 4a shows that the catalysts annealed for 0.5 h, 1h and 2.5 h have almost identical XRD patterns to pc-Ni-Bi@NB (2 h) with all peaks that can be indexed to inner Ni_3B nanocrystals, indicating that finely tuning annealing time can expectedly modulate the crystallinity of outlayer Ni-B_i but does not change the crystal structure of inner Ni_3B nanocrystals. TEM images in Figure 4b-d, Figure S17 (enlarged images), and Figure S18-S21 (more datasets of images) reveal that Ni-B_i outer layer gradually crystallize as annealing. The statistical analysis revealed that the Ni-B_i crystallites sizes in the shell of pc-Ni-B_i@NB-0.5, -2, and -2.5 samples were 2.48, 5.34, and 12.25 nm^2, respectively (Figure S22), corroborating the crystallinity of Ni-B_i shell was increased with the increase of annealing time. Interestingly, significant difference in electrochemical behaviors was clearly observed among these

samples (Figure 4e). The amorphous a-Ni-B_i@NB shows the worst OER activity in terms of the largest overpotential. With the increase of annealing time from 0.5, to 1 and 2 h, the overpotentials at 10 mA cm^{-2} gradually decrease from 341 mV to 328 and 302, implying the initial improvement on the crystallinity of Ni-B_i due to annealing enhances OER activity. However, when the annealing time extends to 2.5, the OER overpotential increases to 322 mV instead, indicating the further improvement on the crystallinity of Ni-B_i downgrades the OER performance. Besides, a pure fully-crystallized sample (c-Ni-B_i) was prepared as an additional control (see supporting information for details). The electrochemical tests show that this fully-crystallized Ni-B_i is less-active for OER (Figure S23). These experiments conclude that the electrocatalytic OER activity of Ni-B_i can be modulated by its crystallinity.

Moreover, it was found that the SSA of the catalysts is increased as the increase of the annealing time (14.9, 15.9, 26.4 and 33.0 m^2 g^{-1} for pc-Ni-Bi@NB-0.5, -1, 2 and -2.5 respectively, Figure S24), which is not directly correlated to the OER performance. Besides the amount of the exposed active sites, the conductivity of the catalysts and the intrinsic activity of the active site may also affect the electrochemical performance. To further unravel the intrinsic activities of catalytic sites, the turnover frequencies (TOF) (Figure 4f) were calculated on a basis of the current integration of Ni^{2+}/Ni^{3+} features on LSV curves which should be directly relevant to the actual amount of catalytic sites in each catalyst. TOF values for all five samples at the overpotential of 300 mV were representatively presented in the inset of Figure 4f. TOF values initially increase as the increase of annealing time and crystallinity of Ni-B_i. The pc-Ni-B_i@NB-2 exhibits the highest TOF value of 0.052 s^{-1}, which is nearly seven times higher than 0.008 s^{-1} for the unannealed a-Ni-B_i@NB. But TOF of pc-Ni-B_i@NB-2.5 decreased to 0.026 s^{-1}. Furthermore, electrochemical impedance spectroscopy (EIS) were measured to further explore the effect of OER kinetics on catalytic activity. As illustrated in Figure S25, all these samples exhibit the similar solution resistances (R_s) at ~ 10.05 ± 0.25 Ω (Table S5) and the slightly changed charge transfer resistances (R_{ct}). As corroborated by the TOF analysis (Figure 4f), we think that the apparent differences in OER activity of Ni-B_i@NB-x samples should mainly originate from the differences in the intrinsic activity of active sites in Ni-B_i with different crystallinity rather than the charge transfer kinetics. It is known that the grain boundaries, point and line defects, undercoordinated sites, and edges at steps or kinks are usually highly reactive and responsible for the enhanced catalytic activity.[24] The partially crystallized Ni-B_i shell in this case was expected to have more such highly reactive sites, leading to the highest OER activity. Therefore, it could be reasonably concluded that the crystallinity of Ni-B_i significantly affects the OER performance of the catalysts by modulating the intrinsic activity of catalytic sites and the partially crystalline Ni-B_i demonstrates the highest OER activity.

In order to give direct evidence on this point, four additional pure nickel (II) borate (Ni-B_i) samples without Ni_3B cores, which can be directly characterized, were prepared and evaluated. The details were presented in the supporting information (Figure S26-28). The results clearly demonstrate the sample with relatively low crystallinity (Ni-B_i-2) exhibits the smallest charge transfer resistance and thus the highest electrocatalytic activity. The sample with highest crystallinity (Ni-B_i-4) shows the largest charge transfer resistance and the lowest electrocatalytic activity. These results indicate that the crystallinity of Ni-B_i does influence the OER activity, well consistent with the above findings on our Ni-B_i@NB catalysts. Moreover, it should be noted that the all pure nickel(II) borate catalysts without Ni_3B cores exhibit worse OER activity than all Ni-B_i@NBs with Ni_3B cores (Figure 4e and Figure S28b), implying that Ni_3B core could play an important role in enhancing OER activity by influencing the Ni-B_i shell like other core-shell electrocatalysts.[25] Actually, the EIS results exhibit that Ni-B_i@NBs have much smaller R_{ct} (1.66 ~ 5.04 Ω, Figure S24) than pure Ni-Bi samples without Ni_3B cores (109 ~ 261 Ω, Figure S27a), indicating the inner Ni_3B cores could facilitate the electron transfer during OER given that the metallic Ni_3B is much more conductive than nickel(II) borate. However, the XPS analyses discover that the variation of Ni^0 amount in all four pc-Ni-B_i@NB-x (x=0.5, 1, 2, and 2.5) samples is within 1 at. %, which should be within the measurement error (Table S4). Since the inner Ni_3B cores were covered by Ni-B_i shell and the four samples have the similar inner Ni_3B cores in both crystalline structure and composition (as demonstrated by XRD and TEM) but show significantly different OER performance, the inner Ni_3B cores should not directly act as active sites for OER. Additionally, as mentioned before in Figure 3b and S14, pure Ni_3B nanoparticles without Ni-B_i shell show appreciably wore OER activity than pc-Ni-B_i@NB (409 mV vs. 302 mV overpotential at 10 mA cm^{-2}). The above results suggested that Ni_3B core could contribute to the enhanced OER activity by influencing the Ni-B_i shell but the Ni-B_i shell is more active and dominates the high OER activity of pc-Ni-B_i@NB.

Besides the high activity, excellent durability is also required for an applicable electrocatalyst. To assess the durability of pc-Ni-B_i@NB, chronopotentiometric measurement at 10 mA cm^{-2} was consecutively performed for 8 h. Figure 4g displays that the overpotential (without iR-correction) keeps steady at 313 mV without detectable deterioration during assessment, which is superior to those of a-Ni-B_i@NB and commercial IrO_2 (Figure S29). HRTEM image (Figure S30) and XPS spectra (Figure S31) clearly demonstrate that the Ni-B_i outlayer on Ni_3B nanoparticles survives after long-term durability test.

In summary, we explored the potential of nickel (II) borate (Ni-B_i) as a new efficient OER electrocatalyst using Ni-B_i@N_3B nanoparticles prepared via a very simple aqueous reaction. The dependence of the OER electrocatalytic activity of Ni-B_i on its crystallinity was first and in-depth investigated. It was interestingly found that the partially crystalline Ni-B_i exhibited the much higher OER activity than amorphous or crystalline one. This will open up opportunities to improve the electrochemical performance of electrocatalysts by delicately modulating its crystallinity. In view of the small overpotential of 302 mV at 10 mA cm^{-2} for OER in 1 M KOH and Tafel slope of 52 mV/decade achieved by the developed pc-Ni-B_i@NB nanoparticles, partially crystalline nickel (II) borates are promising to be a new class of non-precious efficient OER electrocatalysts, especially by fabricating the three-dimensional nanostructures or in combination with other active materials.

Acknowledgements

We acknowledge the financial support from the National Key Project on Basic Research (2015CB932302), the National Key Research and Development Program of China (2016YFB0101202), the National Natural Science Foundation of China (91645123 and 21573249), and the Strategic Priority Research Program of the Chinese Academy of Sciences (Grant No. XDB12020100). We thank Dr. Fen Liu, Dr. Zhijuan Zhao and Xiaoyu Zhang for their help in XPS analysis.

Keywords: oxygen evolution reaction • OER • nickel borate • partially crystalline • electrolysis

[1] I. Katsounaros, S. Cherevko, A. R. Zeradjanin, K. J. J. Mayrhofer, *Angew. Chem. Int. Ed.* **2014**, *53*, 102-121.

[2] a) J. Wang, W. Cui, Q. Liu, Z. Xing, A. M. Asiri, X. Sun, *Adv. Mater.* **2016**, *28*, 215-230; b) D. Chen, C. Chen, Z. M. Baiyee, Z. Shao, F. Ciucci, *Chem. Rev.* **2015**, *115*, 9869-9921; c) X. Deng, H. Tüysüz, *ACS Catal.* **2014**, *4*, 3701-3714; d) F. Jiao, H. Frei, *Energy Environ. Sci.* **2010**, *3*, 1018-1027.

[3] M. Gao, W. Sheng, Z. Zhuang, Q. Fang, S. Gu, J. Jiang, Y. Yan, *J. Am. Chem. Soc.* **2014**, *136*, 7077-7084.

[4] a) C. C. L. McCrory, S. Jung, I. M. Ferrer, S. M. Chatman, J. C. Peters, T. F. Jaramillo, *J. Am. Chem. Soc.* **2015**, *137*, 4347-4357; b) C. C. L. McCrory, S. Jung, J. C. Peters, T. F. Jaramillo, *J. Am. Chem. Soc.* **2013**, *135*, 16977-16987.

[5] a) Y. Li, P. Hasin, Y. Wu, *Adv. Mater.* **2010**, *22*, 1926-1929; b) M. S. Burke, L. J. Enman, A. S. Batchellor, S. Zou, S. W. Boettcher, *Chem. Mater.* **2015**, *27*, 7549-7558; c) M. W. Louie, A. T. Bell, *J. Am. Chem. Soc.* **2013**, *135*, 12329-12337; d) J. Nai, H. Yin, T. You, L. Zheng, J. Zhang, P. Wang, Z. Jin, Y. Tian, J. Liu, Z. Tang, L. Guo, *Adv. Energy Mater.* **2015**, *5*, 1401880; e) F. Song, X. Hu, *Nat. Commun.* **2014**, *5*, 4477; f) L. Kuai, J. Geng, C. Chen, E. Kan, Y. Liu, Q. Wang, B. Geng, *Angew. Chem. Int. Ed.* **2014**, *53*, 7547-7551; g) J. Bao, X. Zhang, B. Fan, J. Zhang, M. Zhou, W. Yang, X. Hu, H. Wang, B. Pan, Y. Xie, *Angew. Chem. Int. Ed.* **2015**, *54*, 7399-7404; h) M. Gong, Y. Li, H. Wang, Y. Liang, J. Z. Wu, J. Zhou, J. Wang, T. Regier, F. Wei, H. Dai, *J. Am. Chem. Soc.* **2013**, *135*, 8452-8455; i) S. Chen, J. Duan, M. Jaroniec, S. Z. Qiao, *Angew. Chem. Int. Ed.* **2013**, *52*, 13567-13570.

[6] a) Z. Peng, D. Jia, A. M. Al-Enizi, A. A. Elzatahry, G. Zheng, *Adv. Energy Mater.* **2015**, *5*, 1402031; b) Y. Liu, C. Xiao, M. Lyu, Y. Lin, W. Cai, P. Huang, W. Tong, Y. Zou, Y. Xie, *Angew. Chem. Int. Ed.* **2015**, *54*, 11231-11235.

[7] a) M.-R. Gao, Y.-F. Xu, J. Jiang, Y.-R. Zheng, S.-H. Yu, *J. Am. Chem. Soc.* **2012**, *134*, 2930-2933; b) C. Tang, N. Cheng, Z. Pu, W. Xing, X. Sun, *Angew. Chem. Int. Ed.* **2015**, *54*, 9351-9355; c) Y. Hou, M. R. Lohe, J. Zhang, S. Liu, X. Zhuang, X. Feng, *Energy Environ. Sci.* **2016**, *9*, 478-483; d) A. T. Swesi, J. Masud, M. Nath, *Energy Environ. Sci.* **2016**; e) C. Xia, Q. Jiang, C. Zhao, M. N. Hedhili, H. N. Alshareef, *Adv. Mater.* **2016**, *28*, 77-85.

[8] a) L.-A. Stern, L. Feng, F. Song, X. Hu, *Energy Environ. Sci.* **2015**, *8*, 2347-2351; b) M. Ledendecker, S. Krick Calderón, C. Papp, H.-P. Steinrück, M. Antonietti, M. Shalom, *Angew. Chem. Int. Ed.* **2015**, *54*, 12361-12365.

[9] a) P. Chen, K. Xu, Z. Fang, Y. Tong, J. Wu, X. Lu, X. Peng, H. Ding, C. Wu, Y. Xie, *Angew. Chem. Int. Ed.* **2015**, *54*, 14710-14714; b) K. Xu, P. Chen, X. Li, Y. Tong, H. Ding, X. Wu, W. Chu, Z. Peng, C. Wu, Y. Xie, *J. Am. Chem. Soc.* **2015**, *137*, 4119-4125.

[10] a) S. Carenco, D. Portehault, C. Boissière, N. Mézailles, C. Sanchez, *Chem. Rev.* **2013**, *113*, 7981-8065; b) S. Gupta, N. Patel, A. Miotello, D. Kothari, *J. Power Sources* **2015**, *279*, 620-625; c) H. Vrubel, X. Hu, *Angew. Chem. Int. Ed.* **2012**, *51*, 12703-12706; d) J. Masa, P. Weide, D. Peeters, I. Sinev, W. Xia, Z. Sun, C. Somsen, M. Muhler, W. Schuhmann, *Adv. Energy Mater.* **2016**, *6*, 1502313.

[11] M. W. Kanan, D. G. Nocera, *Science* **2008**, *321*, 1072-1075.

[12] N. Jiang, B. You, M. Sheng, Y. Sun, *Angew. Chem. Int. Ed.* **2015**, *54*, 6251-6254.

[13] P. Chen, K. Xu, T. Zhou, Y. Tong, J. Wu, H. Cheng, X. Lu, H. Ding, C. Wu, Y. Xie, *Angew. Chem. Int. Ed.* **2016**, *55*, 2488-2492.

[14] M. Dincă, Y. Surendranath, D. G. Nocera, *Proc. Natl. Acad. Sci.* **2010**, *107*, 10337-10341.

[15] a) D. K. Bediako, B. Lassalle-Kaiser, Y. Surendranath, J. Yano, V. K. Yachandra, D. G. Nocera, *J. Am. Chem. Soc.* **2012**, *134*, 6801-6809; b) D. K. Bediako, Y. Surendranath, D. G. Nocera, *J. Am. Chem. Soc.* **2013**, *135*, 3662-3674.

[16] A. Indra, P. W. Menezes, N. R. Sahraie, A. Bergmann, C. Das, M. Tallarida, D. Schmeißer, P. Strasser, M. Driess, *J. Am. Chem. Soc.* **2014**, *136*, 17530-17536.

[17] J. Legrand, S. Gota, M. J. Guittet, C. Petit, *Langmuir* **2002**, *18*, 4131-4137.

[18] G. M. Arzac, T. C. Rojas, A. Fernández, *ChemCatChem* **2011**, *3*, 1305-1313.

[19] P. Zhang, M. Wang, Y. Yang, T. Yao, H. Han, L. Sun, *Nano Energy* **2016**, *19*, 98-107.

[20] a) L. Liu, L. Hong, *Catal. Today* **2016**, *263*, 52-60; b) M. C. López, G. F. Ortiz, P. Lavela, R. Alcántara, J. L. Tirado, *ACS Sustainable Chem. Eng.* **2013**, *1*, 46-56; c) X. Lu, C. Zhao, *Nat. Commun.* **2015**, *6*, 6616.

[21] a) Z. L. Wang, J. S. Yin, W. D. Mo, Z. J. Zhang, *J. Phys. Chem. B* **1997**, *101*, 6793-6798; b) K. Karki, Y. Huang, S. Hwang, A. D. Gamalski, M. S. Whittingham, G. Zhou, E. A. Stach, *ACS Appl. Mater. Interfaces* **2016**, *8*, 27762-27771.

[22] C. Wu, Y. Bai, D.-X. Liu, F. Wu, M.-L. Pang, B.-L. Yi, *Catal. Today* **2011**, *170*, 33-39.

[23] R. Chen, H.-Y. Wang, J. Miao, H. Yang, B. Liu, *Nano Energy* **2015**, *11*, 333-340.

[24] a) L. Bu, S. Guo, X. Zhang, X. Shen, D. Su, G. Lu, X. Zhu, J. Yao, J. Guo, X. Huang, *Nat. Commun.* **2016**, *7*, 11850; b) N. Tian, Z.-Y. Zhou, S.-G. Sun, Y. Ding, Z. L. Wang, *Science* **2007**, *316*, 732-735; c) X. Feng, K. Jiang, S. Fan, M. W. Kanan, *J. Am. Chem. Soc.* **2015**, *137*, 4606-4609; d) M. Li, Z. Zhao, T. Cheng, A. Fortunelli, C.-Y. Chen, R. Yu, Q. Zhang, L. Gu, B. Merinov, Z. Lin, E. Zhu, T. Yu, Q. Jia, J. Guo, L. Zhang, W. A. Goddard, Y. Huang, X. Duan, *Science* **2016**, *354*, 1414.

[25] D. Wang, H. L. Xin, R. Hovden, H. Wang, Y. Yu, D. A. Muller, F. J. DiSalvo, H. D. Abruña, *Nat. Mater.*, **2013**, *12*, 81.

COMMUNICATION

Crystallinity-dependent activity was demonstrated on a new efficient OER electrocatalyst with nickel (II) borate thin layer on nickel boride (NB) nanoparticles (Ni-B_i@NB). The partially crystalline Ni-B_i exhibits the best OER performance with a small overpotential of 302 mV at 10 mA cm^{-2} and a Tafel slope of 52 mV/decade.

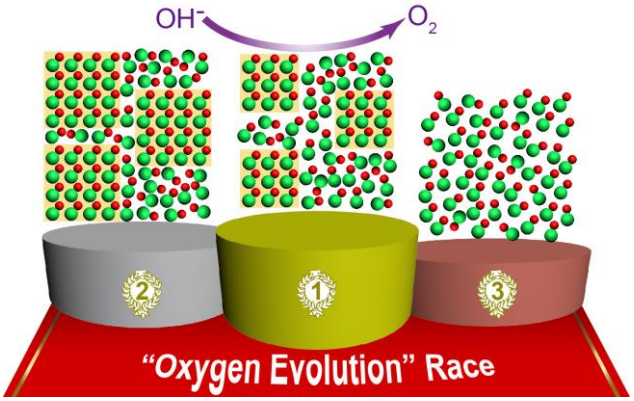

*Wen-Jie Jiang, Shuai Niu, Tang Tang, Yun Zhang, Yu-Yun Chen, Li-Jun Wan, and Jin-Song Hu**

Page No. – Page No.

Crystallinity modulated electrocatalytic activity of nickel(II) borate thin layer on Ni_3B for efficient water oxidation

Author/s:
Jiang, W;Niu, S;Tang, T;Zhang, Q;Liu, X;Zhang, Y;Chen, Y;Li, J;Gu, L;Wan, L;Hu, J

Title:
Crystallinity#Modulated Electrocatalytic Activity of a Nickel(II) Borate Thin Layer on Ni₃B for Efficient Water Oxidation

Date:
2017-06

Citation:
Jiang, W., Niu, S., Tang, T., Zhang, Q., Liu, X., Zhang, Y., Chen, Y., Li, J., Gu, L., Wan, L. & Hu, J. (2017). Crystallinity#Modulated Electrocatalytic Activity of a Nickel(II) Borate Thin Layer on Ni₃B for Efficient Water Oxidation. Angewandte Chemie, 129 (23), pp.6672-6677. https://doi.org/10.1002/ange.201703183.